High-Efficiency Harmonic-Peaking Class-EF Power Amplifiers with Enhanced Maximum Operating Frequency

Mury Thian, Ayman Barakat and Vincent Fusco, *Fellow, IEEE*

***Abstract*—The recently introduced Class-EF power amplifier (PA) has a peak switch voltage lower than that of Class-E PA. However, the value of the transistor output capacitance at high frequencies is typically larger than the required Class-EF optimum shunt capacitance. Consequently, soft-switching operation that minimizes power dissipation during OFF-to-ON transition cannot be achieved at high frequencies. Two new Class-EF PA variants with transmission-line load networks, namely, third-harmonic-peaking (THP) and fifth-harmonic-peaking (FHP) Class-EF PAs are proposed in this paper. These permit operation at higher frequencies at no expense to other PA figures of merit. Analytical expressions are derived in order to obtain circuit component values which satisfy the required Class-EF impedances at fundamental frequency, all even harmonics, and the first few odd harmonics as well as simultaneously providing impedance matching to a 50 Ω load. Furthermore, a novel open-circuit and shorted stub arrangement which has substantial practical benefits is proposed to replace the normal quarter-wave line connected at the transistor's drain. Using GaN HEMTs, two PA prototypes were built. Measured peak drain efficiency of 91% and output power of 39.5 dBm were obtained at 2.22 GHz for the THP Class-EF PA. The FHP Class-EF PA delivered output power of 41.9 dBm with 85% drain efficiency at 1.52 GHz.**

***Index Terms*—Class-E, Class-EF, Class-F, fifth-harmonic-peaking, GaN, HEMT, power amplifiers, third-harmonic-peaking, transmission lines.**

I. Introduction

THE Class-E power amplifier (PA) [1]-[5] theoretically offers 100% DC-to-RF efficiency since its switch voltage and current waveforms are tailored such that they do not overlap each other. It adopts zero voltage switching (ZVS) and zero voltage derivative switching (ZVDS) conditions so as to enable soft-switching operation which minimizes power dissipation during OFF-to-ON transition. However, the peak switch voltage of Class-E PA is considerably high. The Inverse Class-E PA [6]-[8] and Class-F PA [9]-[13] offer substantially lower peak switch voltage than the Class-E counterpart but cannot facilitate soft-switching operation since their idealized circuit topologies do not incorporate a shunt capacitance (C) that is connected in parallel with the switch. In practice, this means that the transistor output capacitance (C_{OUT}) cannot be effectively absorbed. The output capacitance of an actual transistor typically has nonlinear characteristic since it depends on instantaneous drain-source voltage values. The analysis in [14] presented a design methodology for Class-E PA wherein the nonlinear output capacitance can be adequately approximated with an equivalent linear capacitance.

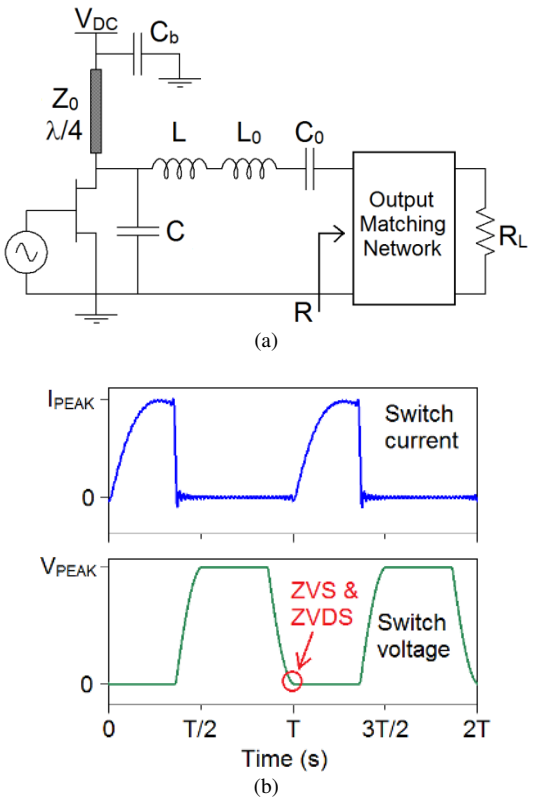

Fig. 1. Class-EF PA with lumped-element load-network: (a) Basic circuit (b) Idealized steady-state switch voltage and current waveforms.

The Class-EF PA and its variants reported in [15]-[20] offer a low peak switch voltage of only $2V_{DC}$ as in the Class F as well as soft-switching operation as in the Class E, Fig. 1.

Manuscript received September 1, 2014; revised November 12, 2014 and December 5, 2014; accepted December 21, 2014. This work was supported by the Northern Ireland Department for Employment and Learning (DEL) under Strengthening All Island Mobile Wireless Futures programme and by the FP7 Marie Curie EID programme under ARTISAN project.

The authors are with the Queen's University of Belfast, ECIT Institute, Queen's Road, Queen's Island, Belfast, BT3 9DT, United Kingdom (e-mail: m.thian@qub.ac.uk).

Further, since the switch voltage has maximally flat peak, Fig. 1(b), the Class-EF PA is relatively immune to the detrimental effects that the nonlinear output capacitance has on its performance.

A major challenge in Class-EF PA design is that for a given output power and DC supply voltage (V_{DC}), the maximum operating frequency (f_{MAX}) is constrained by the transistor output capacitance (C_{OUT}), i.e., at high frequencies the value of C_{OUT} is typically larger than the value of C, Fig. 1(a), that results from the Class-EF synthesis. An external shunt inductance (L_P) can be used to tune out the excess capacitance C_X (= $C_{OUT} - C$) at the fundamental frequency. However, the net reactance of this parallel circuit L_P-C_X at higher harmonics ($2f_0$, $3f_0$, etc.) would be capacitive. As a consequence, the open-circuit requirement at odd harmonics for optimum Class-EF operation would be violated. The theoretical analysis in [20] demonstrates that the f_{MAX} of the Class-EF PA can be increased by reducing the duty ratio, by switching the transistor ON for a shorter period. However, this strategy results in low power-output capability and low load resistance. The fact that large devices with high-power-handling capability are always accompanied with high C_{OUT} would appear to render the Class-EF PA topology unsuitable for high power applications.

In order to address the aforementioned issues, we introduce two new variants of the Class-EF PA, namely third-harmonic-peaking (THP) and fifth-harmonic-peaking (FHP) Class-EF PAs. Synthesized in the frequency domain, these PAs employ a simple transmission-line load network and allow operation at higher f_{MAX}. While the THP Class-EF PA satisfies the open-circuit termination requirement at $3f_0$ alone, the FHP Class-EF PA [21] satisfies the requirement simultaneously at $3f_0$ and $5f_0$. On the other hand, the requirement for short-circuit termination at all even harmonics is satisfied through deployment of a quarter-wave (λ/4) line connected at the drain. Closed-form expressions are analytically derived not only to satisfy the Class-EF load-impedance requirements at the fundamental frequency, all even harmonics, and the first few odd harmonics but also to simultaneously provide an impedance matching to 50-Ω load thus obviating the need for additional output matching circuitry. Since the open-circuit conditions at $3f_0$ and $5f_0$ are satisfied and all even harmonic components are shorted by the λ/4 line, high purity output spectrum can be obtained from the FHP Class-EF PA load network. This relaxes the design specifications for additional filtering typically required at the PA output for compliance with standardized out-of-band emission regulations. Further, when compared to the Class-E_3F and Class E_3F_2 PAs in [20], the new PAs generate a less distorted output signal. In addition, these new PAs employ novel λ/8 open-circuit and shorted stubs which replace the classical λ/4 transmission line (TL). This arrangement offers better open- and short-circuit terminations and has the capability to independently control open- and short-circuit terminations at the transistor's drain, which in turn improve the PA's efficiency.

This paper is organized as follows: basic operation of the Class-EF PA with lumped-element load network along with some design trade-offs awareness is briefly reviewed in Section II. Sections III and IV present the theoretical analysis of the THP and FHP Class-EF PAs, respectively. Circuit design examples and simulations using ideal components are treated in Section V. Finally in Section VI, implementation of the PAs using GaN HEMTs and measurement results are discussed.

II. Review of Class-EF Power Amplifier

The circuit schematic for the Class-EF PA is depicted in Fig. 1(a). The transistor must be driven sufficiently hard such that it operates like a switch rather than a current source. The optimal load impedances at fundamental frequency and higher harmonics seen by the transistor, Z_{OPT}, are given in (1). The load network will present R in series with L at f_0, a short circuit at all even harmonics, and an open circuit at all odd harmonics. For prescribed output power (P_O), DC supply voltage (V_{DC}), and operating frequency (f_0), the optimal load resistance R and series inductance L can be calculated using (2)-(3). The shunt capacitance C may entirely furnish the device output capacitance C_{OUT} and its value is given in (4). Note that in (2)-(4) the parameter named dead time τ_D (in rad) is related to duty ratio D by $D = 0.5 - \tau_D/(2\pi)$. For example, $\tau_D = \pi/2$ rad corresponds to $D = 0.25$ meaning that the transistor will be switched ON for a period of 25% of the full cycle.

A quarter-wave line is employed at the drain of the transistor so as to enforce short-circuit termination at all even harmonics. Steady-state switch voltage and current waveforms of the Class-EF PA are illustrated in Fig. 1(b) and the peak switch voltage is $2V_{DC}$. By substituting $C = C_{OUT}$ into (4), the expression for f_{MAX} can be obtained, (5). P_{MAX} (6a) is defined as a ratio between output power and the product of peak switch voltage and peak switch current (6b).

$$Z_{OPT} = \begin{cases} R + j\omega_0 L & \text{at } f_0 \\ 0 & \text{at } 2nf_0,\ n = 1,2,3,\ldots \\ \infty & \text{at } (2n+1)f_0,\ n = 1,2,3,\ldots \end{cases} \quad (1)$$

$$R = \frac{2\left(1+\cos\tau_D\right)^2}{\pi^2}\frac{V_{DC}^2}{P_O} \quad (2)$$

$$L = \frac{\tau_D - 0.5\sin(2\tau_D)}{\sin^2\tau_D}\frac{R}{\omega_0} \quad (3)$$

$$C = \frac{\pi}{2}\left(\frac{\sin\tau_D}{1+\cos\tau_D}\right)^2\frac{P_O}{\omega_0 V_{DC}^2} \quad (4)$$

$$f_{MAX} = \frac{1}{4}\left(\frac{\sin\tau_D}{1+\cos\tau_D}\right)^2\frac{P_O}{C_{OUT}V_{DC}^2} \quad (5)$$

$$P_{MAX} = \begin{cases} \left(1+\cos\tau_D\right)/(4\pi) & ;\ \tau_D \le \pi/2 \\ \left(1+\cos\tau_D\right)/(4\pi\sin\tau_D) & ;\ \pi/2 < \tau_D < \pi \end{cases} \quad (6a)$$

$$I_{MAX} = \begin{cases} 2I_R & ;\tau_D \le \pi/2 \\ 2I_R \sin\tau_D & ;\pi/2 < \tau_D < \pi \end{cases} \quad (6b)$$

where

$$I_R = \frac{\pi}{1+\cos\tau_D} I_{DC} \quad (6c)$$

III. Third-Harmonic-Peaking Class-EF PA with Enhanced f_{MAX}

A new Class-EF PA circuit topology with transmission-line load network is depicted in Fig. 2. In practice, it is impossible to realize a transmission-line load network that could simultaneously satisfy Class-EF impedance requirements at the fundamental frequency as well as at all even and odd harmonics (1) since this would require an infinite number of transmission lines. However, as will be shown shortly, a good approximation to the idealized Class-EF operation can be achieved by satisfying the required impedances at f_0, all even harmonics, and only the first few odd harmonics. Here, a third-harmonic-peaking (THP) Class-EF PA is proposed wherein the open-circuit requirement is satisfied at $3f_0$ alone. The circuit is also synthesized to simultaneously provide direct impedance matching into a 50-Ω load.

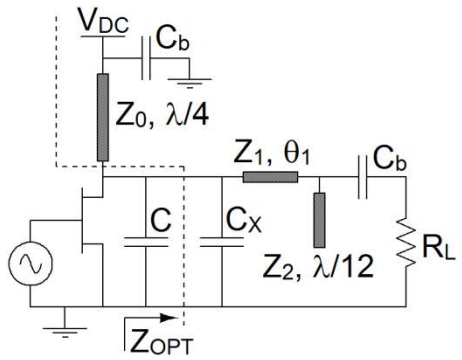

(a)

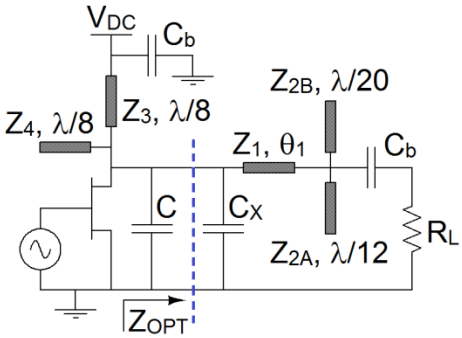

(b)

Fig. 2. Third-harmonic-peaking Class-EF PA with enhanced f_{MAX} employing: (a) λ/4 line, (b) λ/8 open and shorted stubs as well as an additional fifth-harmonic trap TL (Z_{2B}, λ/20).

Enhanced f_{MAX} is achieved by adding extra capacitance C_X to the original Class-EF circuit in Fig. 1(a) and, as a result, the device output capacitance C_{OUT} now increases to $C + C_X$. This translates into higher f_{MAX} expressed in (7) where C_X is defined as kC ($k > 0$).

$$f_{MAX} = \frac{1}{4}\left(\frac{\sin\tau_D}{1+\cos\tau_D}\right)^2 (1+k)\frac{P_O}{C_{OUT}V_{DC}^2} \quad (7)$$

A. Basic Circuit

The electrical length of the open-circuit stub TL_2 in Fig. 2(a) is 90° at $3f_0$ and therefore it provides a short-circuit termination to the series line TL_1. This shorted series line behaves like an inductance (L_1). This inductance must be resonated with C_X in order to provide the required Class-EF open circuit at $3f_0$, hence (8).

$$3\omega_0 C_X \tan(3\theta_1) = Y_1 \quad (8)$$

At the fundamental frequency, the 50 Ω load resistance (R_L) is transformed by TL_1 and TL_2 into an admittance of $1/Z_{OPT}$ - $j\omega_0 C_X$ where Z_{OPT} is given in (1). This results in:

$$G_{OPT} = \frac{G_L Y_1^2 \sec^2\theta_1}{(Y_1 - B_L\tan\theta_1)^2 + G_L^2\tan^2\theta_1} \quad (9)$$

$$\frac{B_{OPT} - \omega_0 C_X}{Y_1} = \frac{(Y_1\tan\theta_1 + B_L)(Y_1 - B_L\tan\theta_1) - G_L^2\tan\theta_1}{(Y_1 - B_L\tan\theta_1)^2 + G_L^2\tan^2\theta_1} \quad (10)$$

where:

$$G_{OPT} = \frac{R}{R^2 + (\omega_0 L)^2} \quad (11)$$

$$B_{OPT} = \frac{-\omega_0 L}{R^2 + (\omega_0 L)^2} \quad (12)$$

$$G_L = 1/R_L = 1/50 \quad (13)$$

$$B_L = Y_2\tan 30^o = Y_2/\sqrt{3} \quad (14)$$

By solving (8)-(10) simultaneously, the values of Z_1 (= $1/Y_1$), θ_1, and Z_2 (= $1/Y_2$) can be obtained. The characteristic impedance of the quarter-wave line Z_0 must be selected sufficiently high so as to isolate the supply voltage from the RF signal. Note that C_b is a DC-blocking capacitance.

B. Modified Load Network

To facilitate for fifth-harmonic suppression, the single open-circuit stub (Z_2, 30°) in Fig. 2(a) is modified into two open-circuit stubs with electrical lengths of 30° and 18°, Fig. 2(b). Their respective characteristic admittances Y_{2A} and Y_{2B} are:

$$Y_{2A} = Y_{2B} = \frac{Y_2\tan 30^o}{\tan 30^o + \tan 18^o} \approx 0.64Y_2 \quad (15)$$

where $Y_{2A} = 1/Z_{2A}$ and $Y_{2B} = 1/Z_{2B}$.

Furthermore, novel λ/8 open-circuit and shorted stubs are now used to replace the traditional λ/4 line. The λ/8 open stub will short circuit the drain of the transistor at $(4m\text{-}2)^{th}$ harmonics whereas the λ/8 shorted stub will short circuit the drain of the transistor at $4m^{th}$ harmonics where m = 1, 2, 3, etc. Together they will facilitate a short-circuit termination at all even harmonics. At the fundamental frequency, the λ/8 shorted stub behaves like an inductance L_3 (16) while the λ/8 open stub behaves like a capacitance C_4 (17). This parallel $L_3 - C_4$ circuit is designed to resonate at f_0 (18).

$$j\omega_0 L_3 = jZ_3 \tan 45^o = jZ_3 \tag{16}$$

$$j\omega_0 C_4 = jY_4 \tan 45^o = jY_4 \tag{17}$$

$$\omega_0^2 L_3 C_4 = 1 \tag{18}$$

Substitution of (16) and (17) into (18) results in:

$$Z_3 = Z_4 \tag{19}$$

By setting Z_3 equal to Z_4, the proposed stub arrangement provides an open circuit not only at f_0 but also at all odd harmonics.

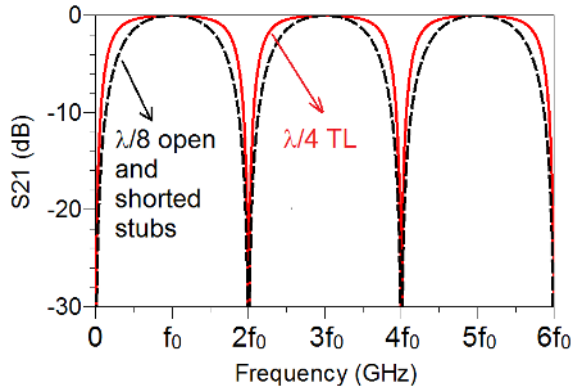

Fig. 3. Characteristics of λ/8 open and shorted stubs vs λ/4 TL.

The bandwidth characteristic of the λ/8 open-circuit and shorted stubs at f_0 and higher harmonics is compared with the λ/4 TL in Fig. 3. It can be observed that the rejection band ($|S21| \leq -10$ dB) of the proposed arrangement is twice as large as that of the λ/4 TL. For illustration, suppose f_0 = 2.5 GHz. The new λ/8 stubs will provide useful attenuation ≥ 10 dB from 4.68 GHz to 5.32 GHz (rejection bandwidth = 640 MHz). At one half these frequencies i.e., from 2.34 GHz to 2.66 GHz (pass-band bandwidth = 320 MHz), insertion loss is better than 0.017 dB. Meanwhile, the traditional λ/4 line will provide the same level of insertion loss i.e., better than 0.017 dB from 2.18 GHz to 2.82 GHz (pass-band bandwidth = 640 MHz i.e., twice as large as that of the λ/8 stubs). However, the rejection levels at 2x these frequencies i.e., from 4.36 GHz to 5.64 GHz are only ≥ 1.875 dB. Therefore it is misleading to conclude that the pass-band bandwidth of the λ/4 line is superior. The correct way to interpret the graph in Fig. 3 is as follows. The λ/4 line will provide attenuation ≥ 10 dB from 4.84 GHz to 5.16 GHz (rejection bandwidth = 320 MHz i.e., one half that of the λ/8 stubs) and this is translated into a pass-band bandwidth of 160 MHz i.e., from 2.42 GHz to 2.58 GHz. In other word, although the insertion loss of the λ/4 line is low across 2.18-2.82 GHz frequency range, only a fraction of this bandwidth i.e., from 2.42 GHz to 2.58 GHz is useful since they result in sufficient rejection levels ≥ 10 dB.

In practice, the λ/4 line in Fig. 2(a) cannot provide ideal short-circuit termination i.e., 0 Ω at even harmonics as required for Class-EF operation due to parasitic resistance ESR. The effect of ESR on the PA efficiency becomes more pronounced in low-voltage high-power designs when the resistance that the supply voltage presents to the PA (R_{DC}) is considerably small. Since the physical length of the λ/8 open and shorted stubs in Fig. 2(b) is just half of that of the λ/4 line, the accompanied ESR will be lower and thus provides better short-circuit termination.

More importantly, the bypass capacitance C_b in Fig. 2 should in theory provide a short circuit at the fundamental frequency as well as at all even and odd harmonics. However, in practice, one capacitor can only be used to provide low impedance (typically around 1 Ω) at a single frequency. For example, in order to provide a short circuit at f_0 and higher harmonics up to $6f_0$, six capacitors are needed. In contrast, the PA in Fig. 2(b) only needs four capacitors since the short-circuit terminations at the drain at $2f_0$ and $6f_0$ are enforced by the λ/8 open-circuit stub and therefore no capacitors are required. Another practical advantage is that the λ/8 open stub will present lower impedance (close to 0 Ω) at the drain resulting in better 2^{nd} and 6^{th} harmonics suppression than when λ/4 TL and C_b are used.

In addition, when implemented in IC format particularly at millimeter-wave frequencies, the proposed stub arrangement offers more flexibility and superior performance than the traditional λ/4 line. In theory a shorted λ/4 line can provide short-circuit termination at all even harmonics. In reality, the length of this line can be effectively tuned at just one frequency (typically $2f_0$) so as to provide the required low-impedance termination. In the proposed stub arrangement, the lengths of the λ/8 open and shorted stubs can be tuned independently to provide low-impedance termination at $2f_0$ and $4f_0$, respectively.

IV. Fifth-Harmonic-Peaking Class-EF PA with Enhanced f_{MAX}

The circuit schematic for the fifth-harmonic-peaking (FHP) Class-EF PA is depicted in Fig. 4. Here, the Class-EF open-circuit requirement is satisfied for the first two odd harmonics, i.e., $3f_0$ and $5f_0$ rather than just $3f_0$ as in the THP Class-EF PA. As a result it mimics idealized Class-EF operation more closely than the THP Class-EF PA. The FHP Class-EF PA is comprised of λ/8 open and shorted stubs which enforce short-circuit terminations at even harmonics, C_X as a means to enhance f_{MAX}, two series transmission lines (TL_1, TL_4), three open-circuit stubs (TL_2, TL_5, TL_6), and a shorted stub (TL_3). In the analysis below, Z_N, Y_N (=$1/Z_N$) and θ_N are, respectively, the characteristic impedance, the characteristic admittance,

and the electrical length of TL_N. Note that C_b is a DC-blocking capacitance and also has a role in preventing the DC signal from being shorted by TL_3.

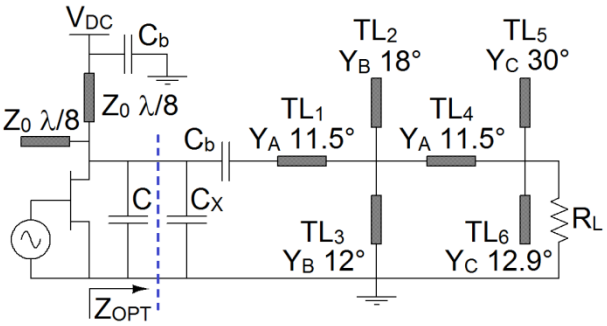

Fig. 4. Fifth-harmonic-peaking Class-EF PA with enhanced f_{MAX} employing λ/8 open and shorted stubs and an additional seventh-harmonic trap TL_6

Consider now the following: TL_6 in Fig. 4 is absent, $\theta_2 = 18°$ and $\theta_5 = 30°$.

At $\mathbf{5}f_0$, the right-hand end of TL_1 will be shorted by TL_2. Provided $\theta_1 < 18°$, the shorted TL_1 will act like an inductance L_1 given in (20). This inductance is designed to resonate with C_X at $5f_0$ so as to provide the required Class-EF odd-harmonic open-circuit condition (21).

$$j5\omega_0 L_1 = jZ_1 \tan(5\theta_1) \tag{20}$$

$$(5\omega_0)^2 L_1 C_X = 1 \tag{21}$$

Substitution of (20) into (21) results in:

$$Y_1 = 5\omega_0 C_X \tan(5\theta_1) \tag{22}$$

At $\mathbf{3}f_0$, TL_2 and TL_3 behave respectively like a capacitance C_2 and an inductance L_3, (23)-(24). This parallel circuit is designed to resonate at $3f_0$ and therefore present an open circuit, (25). As a consequence, TL_1 and TL_4 are now in series connection.

$$j3\omega_0 C_2 = jY_2 \tan 54^o \tag{23}$$

$$j3\omega_0 L_3 = jZ_3 \tan(3\theta_3) \tag{24}$$

$$(3\omega_0)^2 L_3 C_2 = 1 \tag{25}$$

Suppose $Z_2 = Z_3 = Z_B$. Substitution of (23) and (24) into (25) yields:

$$\tan(3\theta_3)\tan 54^o = 1 \tag{26}$$

$$\theta_3 = 12^o \tag{27}$$

On the other hand, the right-hand end of TL_4 will be shorted by TL_5. Provided that $\theta_1 + \theta_4 < 30°$, TL_1 together with the shorted TL_4 will behave like an inductance L_X and this inductance is designed to resonate with C_X at $3f_0$, facilitating an open circuit; see (28)-(29) with $Z_1 = Z_4 = Z_A$. From (28) and (29), we obtain (30).

$$j3\omega_0 L_X = jZ_A \tan\{3(\theta_1 + \theta_4)\} \tag{28}$$

$$(3\omega_0)^2 L_X C_X = 1 \tag{29}$$

$$Y_1 = Y_4 = Y_A = 3\omega_0 C_X \tan\{3(\theta_1 + \theta_4)\} \tag{30}$$

Substitution of (22) into (30) results in:

$$3\tan\{3(\theta_1 + \theta_4)\} = 5\tan(5\theta_1) \tag{31}$$

$$\theta_A = \theta_1 = \theta_4 = 11.535^o \tag{32}$$

With $C_X = C_{OUT} - C$, the characteristic admittance of TL_1 and TL_4, Y_A, can be computed from either (22) or (30).

At $\boldsymbol{f_0}$, $TL_1 - TL_5$ together with C_X will transform the load resistance R_L into $R + j\omega_0 L$. This results in two equations (33)-(34) with two unknown parameters Y_B (= $Y_2 = Y_3$) and Y_5 which can be solved numerically. Note that R and L in (35)-(36) are given in (2)-(3).

$$G_{OPT} = \frac{G_{IN2}\, Y_A^2 \sec^2\theta_A}{(Y_A - B_{IN2}\tan\theta_A)^2 + G_{IN2}^2 \tan^2\theta_A} \tag{33}$$

$$\frac{B_{OPT} - \omega_0 C_X}{Y_A} = \frac{(Y_A \tan\theta_A + B_{IN2})(Y_A - B_{IN2}\tan\theta_A) - G_{IN2}^2 \tan\theta_A}{(Y_A - B_{IN2}\tan\theta_A)^2 + G_{IN2}^2 \tan^2\theta_A} \tag{34}$$

where:

$$G_{OPT} = \frac{R}{R^2 + (\omega_0 L)^2} \tag{35}$$

$$B_{OPT} = \frac{-\omega_0 L}{R^2 + (\omega_0 L)^2} \tag{36}$$

$$G_{IN2} = G_{IN1} \tag{37}$$

$$B_{IN2} = B_{IN1} + Y_B(\tan 18^o + \cot 12^o) \tag{38}$$

and

$$G_{IN1} = \frac{G_L\, Y_A^2 \sec^2\theta_A}{(Y_A - B_L\tan\theta_A)^2 + G_L^2 \tan^2\theta_A} \tag{39}$$

$$\frac{B_{IN1}}{Y_A} = \frac{(Y_A \tan\theta_A + B_L)(Y_A - B_L\tan\theta_A) - G_L^2\tan\theta_A}{(Y_A - B_L\tan\theta_A)^2 + G_L^2\tan^2\theta_A} \tag{40}$$

here:

$$G_L = 1/50 \tag{41}$$

$$B_L = Y_5 \tan 30^o = Y_5/\sqrt{3} \tag{42}$$

Once Y_5 is obtained, a simple modification can be made to facilitate 7th harmonic component suppression by adding an open-circuit stub TL_6 (Y_6, 12.9°) in parallel with TL_5, Fig. 4. For simplicity, we can assume $Y_{5\_new} = Y_6 = Y_C$ and its value

can be calculated using the following formula.

$$Y_C = \frac{Y_5 \tan 30^o}{\tan 30^o + \tan 12.9^o} \approx 0.72 Y_5 \quad (43)$$

V. Design and Simulation Using Ideal Components

Design examples of the THP and FHP Class-EF PAs with enhanced f_{MAX} are now presented in order to better understand the theoretical analysis described in the previous sections. A dead time parameter $\tau_D = 48.5°$ is chosen in order to obtain P_{MAX} 35% higher than that of the Class-E as discussed in Section II. The results presented below were obtained from Keysight Advanced Design Systems (ADS) harmonic-balance simulations using ideal components, i.e., the transmission lines were assumed lossless, the transistor was modeled as a switch with 1 mΩ ON resistance, 10 MΩ OFF resistance, and instantaneous switching time, and was driven by a sine wave.

A. Third-harmonic-peaking Class-EF PA

The design objectives are set as follows: $V_{DC} = 28$ V and $P_O = 10$ W. The transistor which will be used in implementation is a CGH40010F GaN HEMT from CREE with $C_{OUT} = 1.3$ pF. Substituting these values into (5) results in $f_{MAX} = 0.5$ GHz, meaning that the maximum frequency at which the original Class-EF PA in Fig. 1 can be effectively operated is only 0.5 GHz.

Consider now the circuit in Fig. 2. Given $f_0 = 2.5$ GHz, the value of the shunt capacitance C computed using (4) is 0.26 pF. Since $C_{OUT} = 1.3$ pF, the excess capacitance C_X (= C_{OUT} − C) required is 1.04 pF, implying $k = 4$ i.e., f_{MAX} is increased from 0.5 GHz to 2.5 GHz. The transmission-line parameter values Z_1, θ_1, and Z_2 in Fig. 2(a) can be obtained by solving (8)-(10) simultaneously. R and L in (11) and (12) are computed using (2)-(3). The characteristic impedances Z_{2A} and Z_{2B} in Fig. 2(b) can be subsequently determined using (15) and when compared to Z_2 their values are higher. The value of Z_0 must be selected as high as the practical implementation will allow. Here it is set to 80 Ω as values higher than this may result in an impractically narrow microstrip line. The optimal circuit component values are summarized in Table I. The simulated load impedances at the fundamental, second-, and third-harmonic frequencies, Z_{OPT}, are plotted in Fig. 5. In accordance with (1)-(3), the Class-EF mode requirements for short- and open-circuit terminations at $2f_0$ and $3f_0$ respectively are met concurrently, as is the optimal impedance at f_0.

TABLE I
Optimal Circuit Component Values of
the Third-Harmonic-Peaking Class-EF PA, Fig. 2
(2.5 GHz, 28 V, 10 W)

C	0.26 pF	$Z_3 = Z_4$	80 Ω
C_X	1.04 pF	θ_1	69°
Z_1	41 Ω	$\theta_2 = \theta_{2A}$	30°
Z_2	19 Ω	θ_{2B}	18°
$Z_{2A} = Z_{2B}$	29.8 Ω	$\theta_3 = \theta_4$	45°

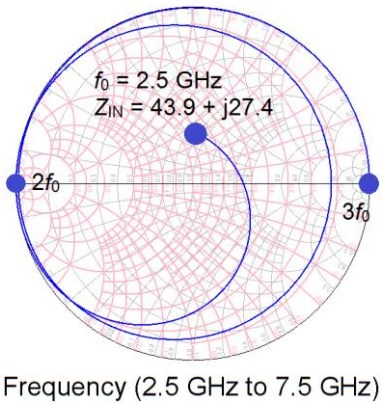

Fig. 5. Simulated load impedances of the THP Class-EF PA at fundamental, second, and third harmonic frequencies.

The effect that the parameter k has on the circuit component values is studied in Fig. 6. As k increases, the values of Z_2 and θ_1 decrease whereas the value of Z_1 remains relatively flat up to $k = 2$ above which it starts to descend. Intuitively, this can be explained as follows. At $3f_0$, the shorted TL_1 behaves like an inductance. This inductance must resonate with C_X so as to provide an open circuit. As k (and accordingly C_X) increases, the shorted TL_1 needs to provide a smaller inductance so as to preserve the resonance at $3f_0$. This is achieved through reduction of Z_1 or θ_1, (8). At $k = 2$, the value of θ_1 has readily descended close to 60° below which $\tan(3\theta_1)$ in (8) would result in negative values, thereby violating (8). As a consequence, for $k > 2$, the slope of θ_1 in Fig. 6 needs to settle, and in order to compensate for this, Z_1 must be accordingly reduced.

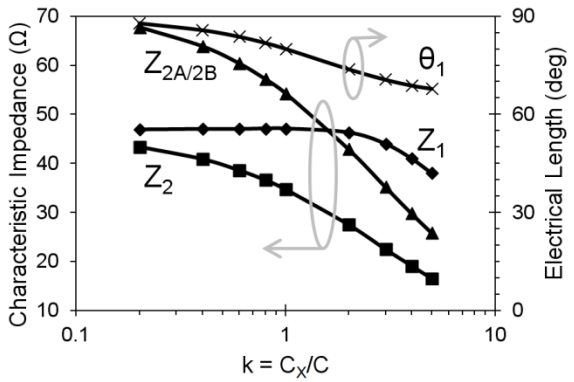

Fig. 6. Optimal transmission-line parameter values versus k of the THP Class-EF PA.

The steady-state voltage and current waveforms of the circuits in Fig. 2 are illustrated in Fig. 7. As can be observed, the ZVS and ZVDS conditions are satisfied during the OFF-to-ON transition. Further, consistent with the theory, the maximally flat peak switch voltage (V_{SW}) of $2V_{DC} = 56$ V is obtained. The currents through the switch and the capacitance C_{OUT} are denoted respectively as I_{SW} and I_{Cout}. Within the interval where V_{SW} is kept constant at $2V_{DC}$, I_{Cout} is zero since I_{Cout} is proportional to the first derivative of V_{SW}. This distinctive feature differentiates the Class-EF PA from the

Class-E PA in which I_{Cout} has non-zero values throughout the OFF interval. Simulated output power and DC current are 39.76 dBm and 340 mA leading to a drain efficiency of 99.5%.

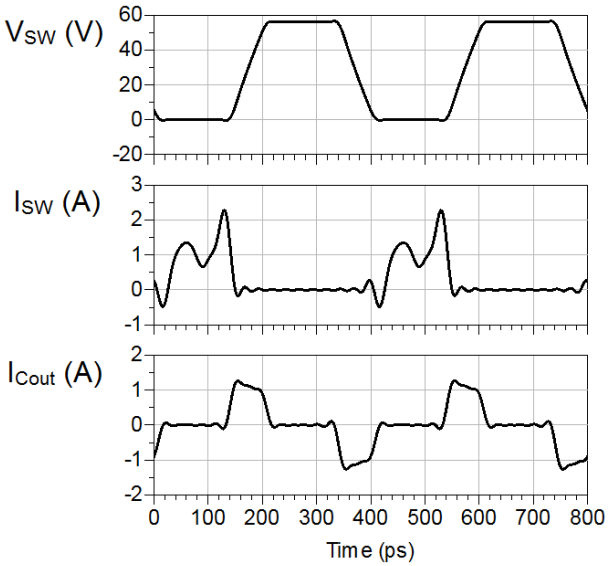

Fig. 7. Steady-state voltage and current waveforms of the THP Class-EF PA (Fig. 2), for $k = 4$.

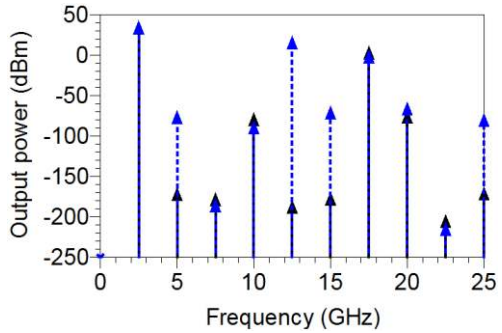

Fig. 8. Simulated output power spectrum of the THP Class-EF PA up to $10f_0$ using ideal components: dotted lines for Fig. 2(a) and solid lines for Fig. 2(b).

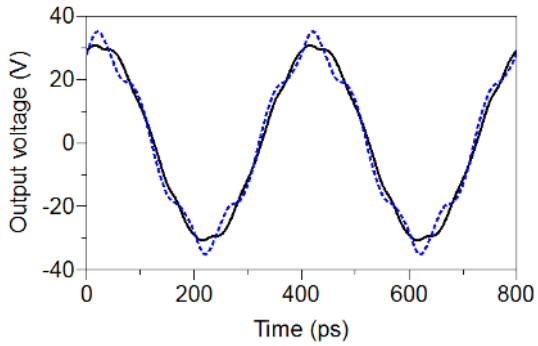

Fig. 9. Output voltage comparison: dotted lines for Fig. 2(a) and solid lines for Fig. 2(b).

Shown in Fig. 8 is the output power spectrum of the PA circuits in Figs. 2(a) and (b). Both PAs are able to deliver the fundamental output power level as specified earlier. TL_{2B} adopted in Fig. 2(b) proves effective as a means to suppress the fifth-harmonic level. As a result, as can be seen from Fig. 9, the output voltage of the PA in Fig. 2(b) looks less distorted than that of Fig. 2(a). The second-, sixth-, and tenth-harmonic component levels of the PAs in Fig. 2(a) and (b) should theoretically be identical – discrepancies shown in Fig. 8 are mainly due to numerical artifacts in ADS.

B. *Fifth-Harmonic-Peaking Class-EF PA*

Consider now the circuit in Fig. 4. The design objectives are set as follows: $f_0 = 2$ GHz, $V_{DC} = 28$ V and $P_O = 13$ W. The value of the shunt capacitance C computed using (4) is 0.42 pF. Since $C_{OUT} = 1.3$ pF, the excess capacitance C_X (= $C_{OUT} - C$) required is 0.88 pF, implying $k \approx 2$ i.e., f_{MAX} is increased from 647 MHz to 2 GHz. Three parameters, i.e., Y_A, Y_B, and Y_C are to be determined. First, the characteristic admittance of TL_1 and TL_4 i.e., Y_A is computed from either (22) or (30) where the value of $\theta_1 = \theta_4$ is given in (32). By simultaneously solving (33) and (34), the values of Y_B and Y_5 can be obtained, and subsequently the value of Y_C is calculated using (43). The optimal circuit component values are summarized in Table II. The simulated load impedances at fundamental and higher harmonic frequencies (up to $5f_0$), Z_{OPT}, are plotted in Fig. 10. In accordance with (1)-(3), the Class-EF mode requirements for short- and open-circuit terminations at even and odd harmonics respectively are satisfied, and so is the optimal impedance at f_0.

TABLE II
OPTIMAL CIRCUIT COMPONENT VALUES OF
THE FIFTH-HARMONIC-PEAKING CLASS-EF PA, FIG. 4
(2 GHz, 28 V, 13 W)

C	0.42 pF	θ_0	45°
C_X	0.88 pF	$\theta_1 = \theta_4$	11.5°
Z_0	80 Ω	θ_2	18°
$Z_1 = Z_4$	23.9 Ω	θ_3	12°
$Z_2 = Z_3$	71.7 Ω	θ_5	30°
$Z_5 = Z_6$	33.2 Ω	θ_6	12.9°

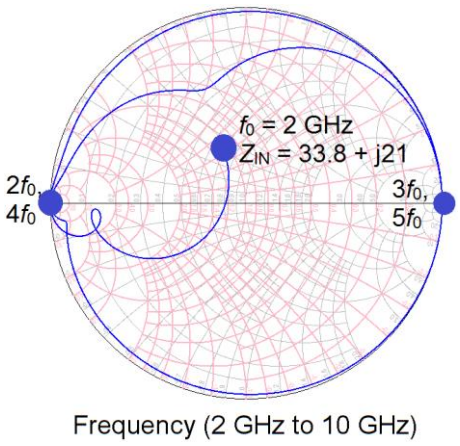

Fig. 10. Simulated load impedances of the FHP Class-EF PA at fundamental and higher harmonic frequencies.

The steady-state voltage and current waveforms are illustrated in Fig. 11. Simulated output power is 12.9 W and simulated DC current is 461 mA, leading to a drain efficiency

of 99.9%. The output power spectrum of the PA circuit in Fig. 4 is shown in Fig. 12 where harmonics up to the 10th are well suppressed. The 2nd, 6th, and 10th harmonic components are suppressed through short-circuit termination facilitated by the λ/8 open-circuit stub. The 4th and 8th harmonic components are suppressed by means of short-circuit termination facilitated by the λ/8 shorted stub. The 3rd and 5th harmonic components are suppressed through open-circuit termination facilitated by the PA's load network i.e., C_X, TL_1-TL_6, and λ/8 open-circuit and shorted stubs. TL_6 is responsible for providing a short-circuit termination to the 7th harmonic component. As a result, the PA produced a nearly pure sine wave at the output (V_O), Fig. 11.

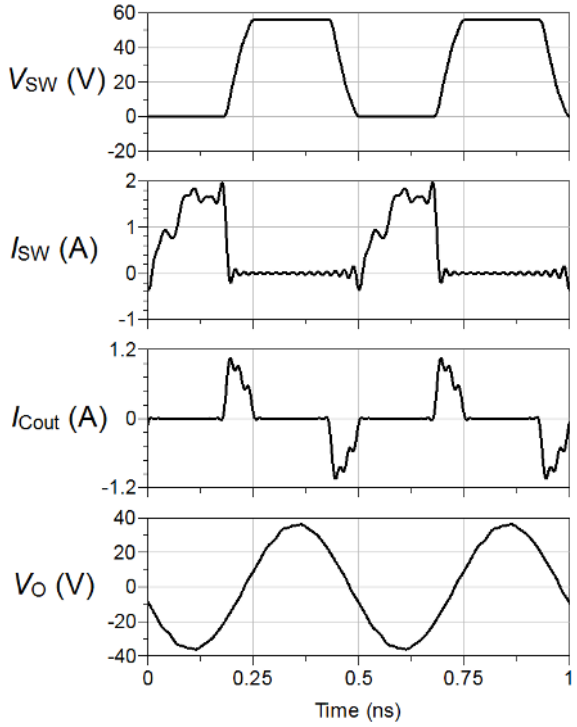

Fig. 11. Steady-state voltage and current waveforms of the FHP Class-EF PA (Fig. 4).

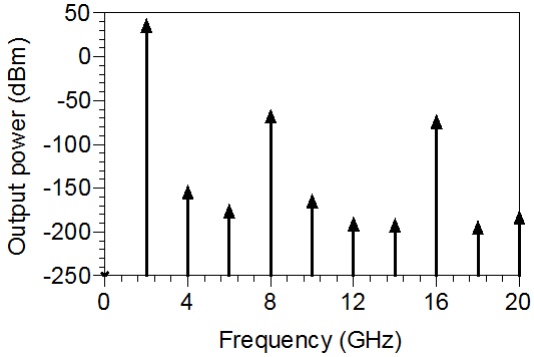

Fig. 12. Simulated output power spectrum of the FHP Class-EF PA up to $10f_0$ using ideal components.

VI. Implementation and Measurement

In order to validate the theoretical synthesis approach in Section III, we fabricated a test board, Fig. 13(a). This comprised of a λ/8 open-circuit stub, a λ/8 shorted stub, and a 50 Ω series TL which connects the input and output ports. The characteristic impedance of the stubs is 80 Ω. The physical dimensions of the stubs are $W = 0.46$ mm and $L = 9.34$ mm. For comparison, another test board comprised of a λ/4 TL ($W = 0.46$ mm and $L = 18.68$ mm) was built, Fig. 13(b). The measured and simulated frequency responses of the stubs at $f_0 = 2.5$ GHz and higher harmonics are compared with the λ/4 TL in Fig. 13(c). It can be observed that the rejection band (|S21| ≤ –10 dB) of the proposed arrangement is as predicted i.e., twice as wide as the λ/4 TL.

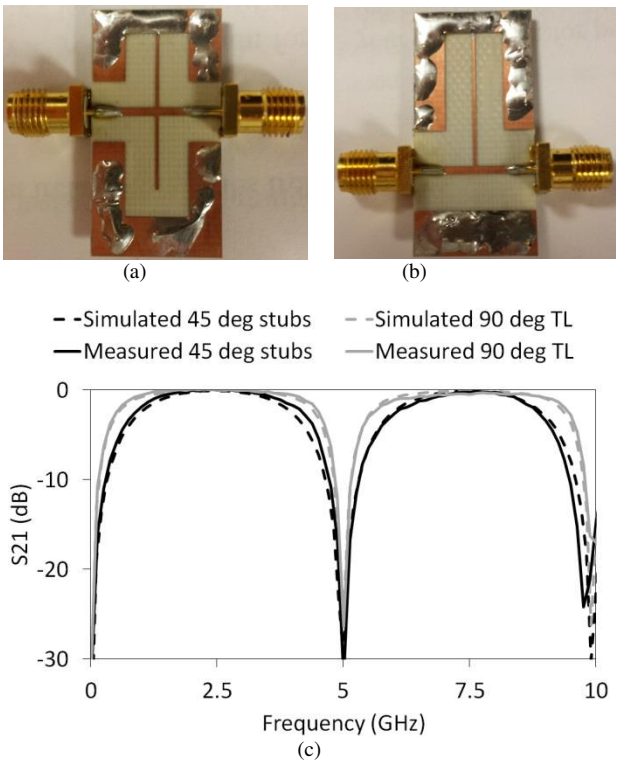

Fig. 13. (a) Test board of the proposed λ/8 stubs, (b) test board of the traditional λ/4 TL, and (c) measured and simulated frequency responses.

For the validation of the THP and FHP Class-EF PAs analysis described in Sections III and IV, two prototypes were built. The PAs employ packaged GaN HEMTs CGH40010F from CREE with drain-source breakdown voltage of 120 V and typical saturated power of 13 W. The manufacturer datasheet shows that the transistor is potentially unstable at frequencies below 3.5 GHz and therefore stabilizing resistors are needed. The PAs were realized on a 0.5-mm thick Rogers RO4003C substrate with dielectric constant of 3.55, loss tangent of 0.0027, and thermal conductivity of 0.71 W/m/°K.

A. *Third-Harmonic-Peaking Class-EF PA*

The circuit component values were initially obtained by converting the characteristic impedance (Z_N) and electrical length (θ_N) values given in Table I into the corresponding microstrip physical dimensions in terms of width (W_N) and length (L_N). These values were then optimized in the simulation in order to give best performances in terms of efficiency, output power and harmonic suppression levels.

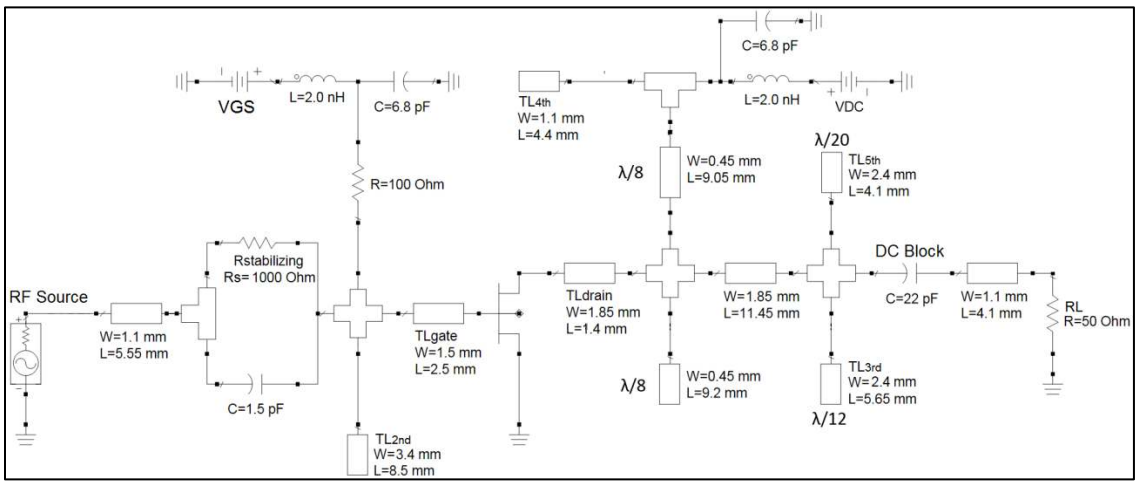

Fig. 14. Complete circuit schematic of the THP Class-EF PA.

TABLE III
TRANSMISSION-LINE LOAD-NETWORK PARAMETER VALUES OF THE THIRD-HARMONIC-PEAKING CLASS-EF PA, FIG. 2(b)
(2.5 GHz, 28 V, 10 W)

Parameter	Theoretical Values (mm)	Optimized Values (mm)
W_1	1.52	1.85
L_1	13.64	11.45
W_{2A}	2.38	2.4
L_{2A}	5.81	5.65
W_{2B}	2.38	2.4
L_{2B}	3.49	4.1
$W_3 = W_4$	0.46	0.45
L_3	9.34	9.05
L_4	9.34	9.2

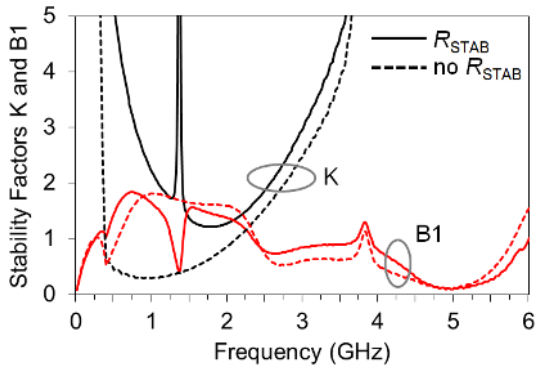

Fig. 15. Simulated stability factors K and B1 before and after adding a stabilizing parallel resistor of 1 kΩ at the input.

The theoretical and optimized circuit component values are presented in Table III.

The complete circuit schematic of the THP Class-EF PA which includes the input matching network, biasing and stabilizing circuits is illustrated in Fig. 14. A 6.8 pF capacitor is used as an RF bypass capacitance as it presents low impedance at the fundamental frequency. The input matching circuit consists of a 1.5 pF series capacitance and an open-circuit stub (TL_{2nd}). A 1 kΩ resistor connected in parallel with the 1.5 pF capacitance is used to make the PA unconditional stable i.e., K is larger than 1 and B_1 is larger than 0, Fig. 15. The photograph of the PA prototype with a square dimension of 4.2 cm × 4.2 cm is depicted in Fig. 16.

As depicted in Fig. 17, a Keysight E8257D signal generator was used to excite the amplifier with a continuous-wave (CW) signal and the output power was measured using Keysight N9320A spectrum analyzer. Since the maximum output power of the signal generator was limited to 17 dBm, an identical replica of the amplifier was used as a driver. A 20-dB attenuator was inserted between the PA and the spectrum analyzer. Gate and drain biasing was applied using Thurlby Thandar power supplies (32 V – 3 A).

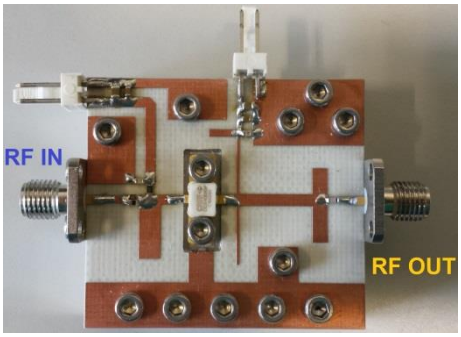

Fig. 16. The THP Class-EF PA prototype.

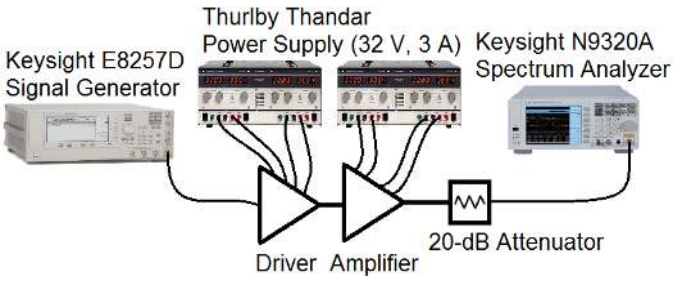

Fig. 17. Measurement setup.

Fig. 18 shows measured output power, gain, drain efficiency and PAE versus input power at 2.22 GHz with $V_{GS} = -2.7$ V and $V_{DC} = 28$ V. Best efficiency performance

i.e., when drain efficiency and PAE peaked at 91% and 80% respectively was achieved at output power of 39.5 dBm and gain of 9.2 dB. At this operating point, 350 mA DC current was drawn from the power supply.

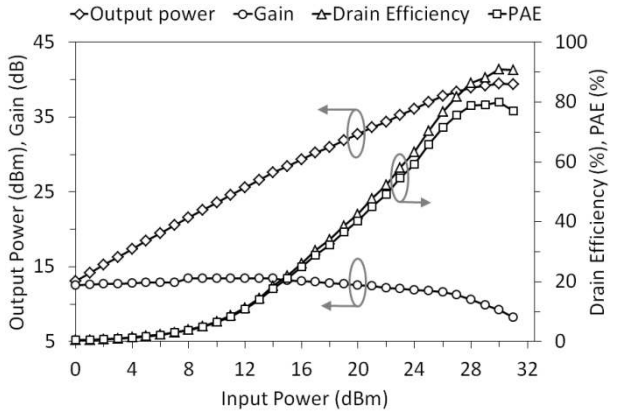

Fig. 18. Measured PA performances versus input power at 2.22 GHz with V_{DC} = 28 V and V_{GS} = -2.7 V.

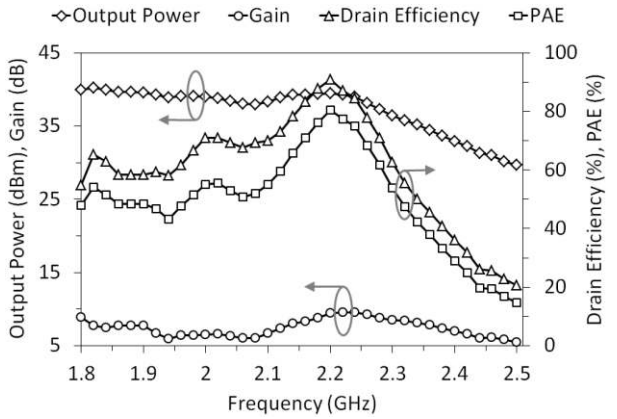

Fig. 19. Measured PA performances versus frequency at V_{DC} = 28 V and V_{GS} = -2.7 V.

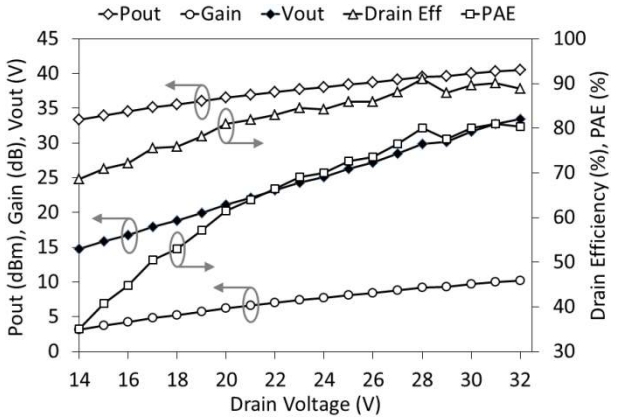

Fig. 20. Measured PA performances versus V_{DC} at 2.22 GHz with V_{GS} = -2.7 V.

The frequency behavior of the PA is illustrated in Fig. 19. Within 460 MHz frequency range i.e., from 1.82 to 2.28 GHz, the PA was able to deliver 38.8±1.5 dBm output power with drain efficiency of at least 58%. PA performance at 2.22 GHz when the supply voltage V_{DC} was swept is shown in Fig. 20. Results show that drain efficiency and PAE remained above 81% and 62% respectively when V_{DC} was varied from 20 to 32 V. Fig. 20 also shows a near linear relationship between output voltage and V_{DC}. This feature is useful for effective deployment of the PA in envelope elimination and restoration (EER) systems or polar transmitters. By decreasing V_{DC} from 28 to 14 V, the output power was reduced by around 6 dB from 39.5 to 33.4 dBm, within which range the drain efficiency remained above 68%. Simulated output power spectrum is shown in Fig. 21.

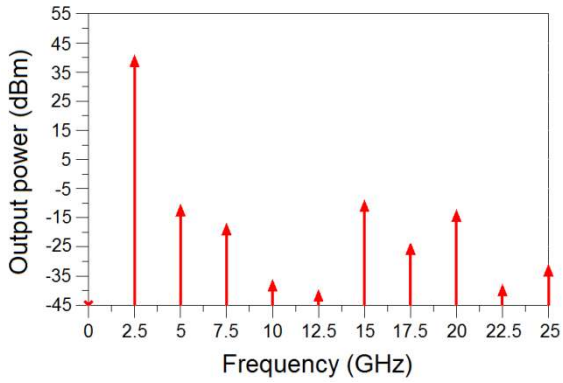

Fig. 21. Simulated output power spectrum of the THP Class-EF PA.

B. *Fifth-Harmonic-Peaking Class-EF PA*

Initial circuit component values were obtained by converting the characteristic impedance (Z_N) and electrical length (θ_N) values given in Table II into the corresponding microstrip physical dimensions i.e., width (W_N) and length (L_N). These values were then optimized in the simulation in order to give best performances in terms of efficiency, output power and harmonic suppression levels. The theoretical and optimized component values are presented in Table IV.

TABLE IV
TRANSMISSION-LINE LOAD-NETWORK PARAMETER VALUES OF THE FIFTH-HARMONIC-PEAKING CLASS-EF PA, FIG. 4
(2 GHz, 28 V, 13 W)

Parameter	Theoretical Values (mm)	Optimized Values (mm)
$W_1 = W_4$	3.17	3.17
$L_1 = L_4$	2.75	2.75
$W_2 = W_3$	0.58	0.58
L_2	4.63	4.5
L_3	3.09	3.09
$W_5 = W_6$	2.06	2.06
L_5	7.31	7.45
L_6	3.13	3
W_0	0.46	0.46
L_{0_short}	11.67	10.5
L_{0_open}	11.67	11.5

The circuit schematic of the FHP Class-EF PA is shown in Fig. 22. The PA employs a simple L-type input matching network comprised of a series capacitance 1.8 pF and a 6.05-mm-long shorted stub. Due to high quality factor (Q) of the

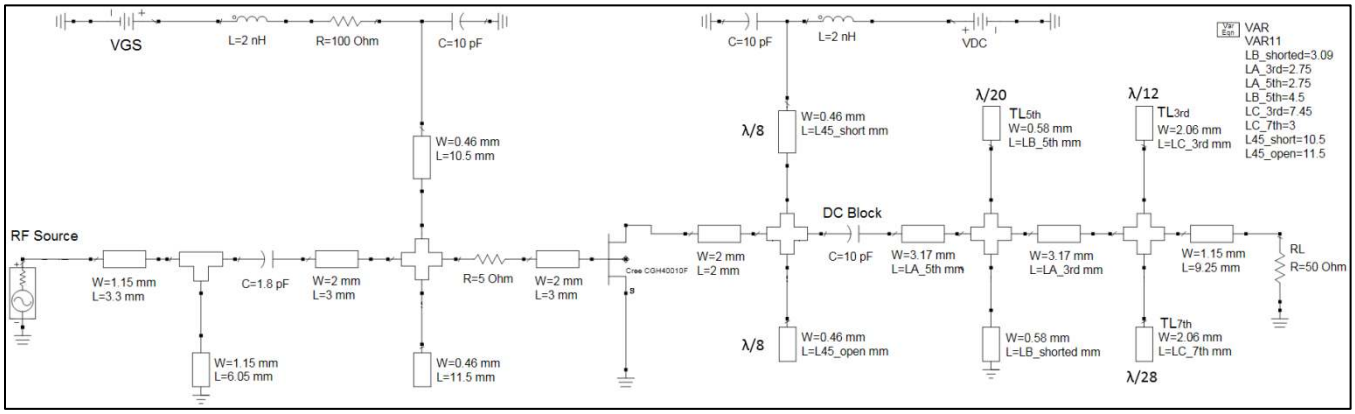

Fig. 22. Complete circuit schematic of the FHP Class-EF PA.

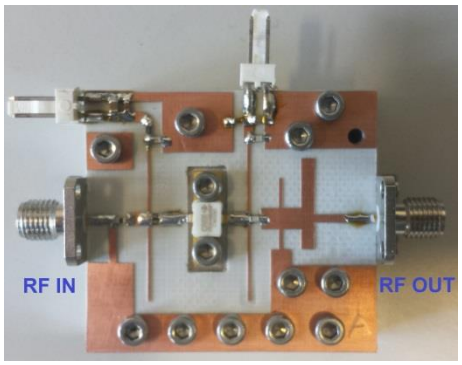

Fig. 23. The FHP Class-EF PA prototype.

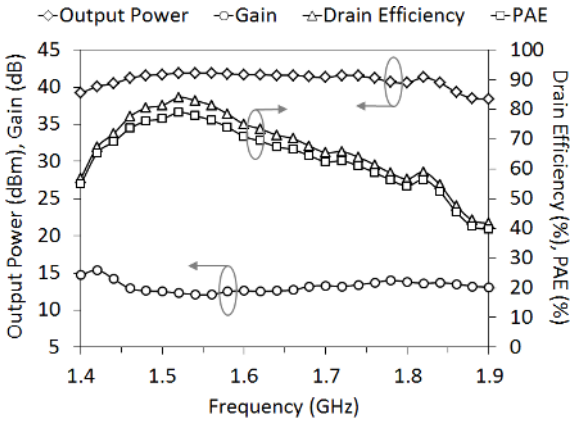

Fig. 24. Measured PA performances versus frequency at V_{DC} = 32 V and V_{GS} = -2.8 V.

complex load network, the FHP Class-EF PA circuit tends to be more sensitive to instability than the THP Class-EF PA. Consequently, a 5-Ω series resistance connected to the transistor's gate was required in order to prevent oscillation, but this comes at the expense of increased power loss. The prototype measures 4 cm × 4 cm, Fig. 23.

Measured PA performances in terms of output power, gain, drain efficiency and PAE at V_{DC} = 32 V and V_{GS} = -2.8 V are plotted against frequency in Fig. 24. Across a 300 MHz frequency range from 1.42 to 1.72 GHz, the PA delivered output power >40 dBm with drain efficiency >65% and PAE >62%. Plotted in Fig. 25 are the measured PA performances

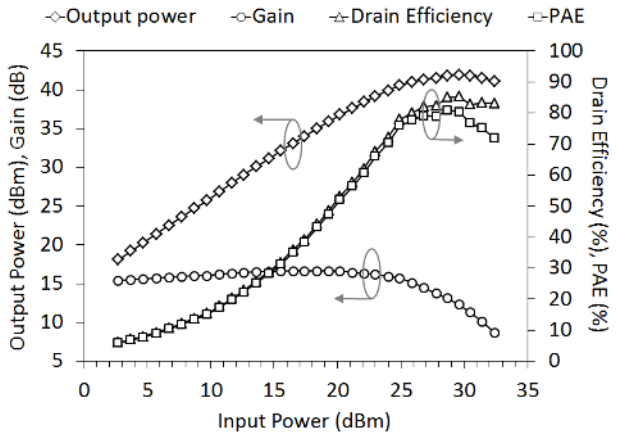

Fig. 25. Measured PA performances versus input power at 1.52 GHz with V_{DC} = 32 V and V_{GS} = -2.8 V.

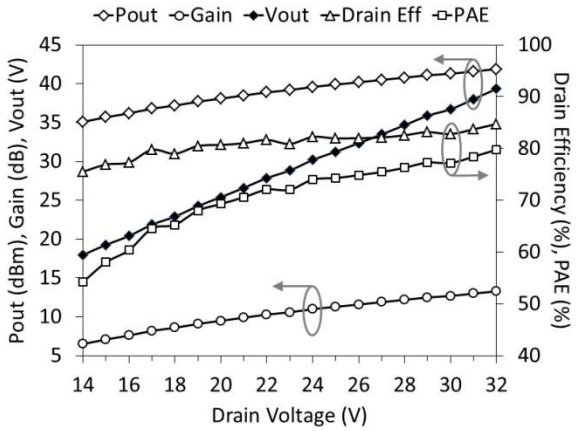

Fig. 26. Measured PA performances versus V_{DC} at 1.52 GHz.

versus input power at 1.52 GHz. Peak drain efficiency of 85% and peak PAE of 81% were achieved at 41.9 dBm output power and 13.1 dB gain. The efficiency is lower than that of the THP Class-EF PA partly due to the 5-Ω series resistor used to stabilize the PA (as opposed to the 1-kΩ parallel resistor used in the THP Class-EF PA). The linear gain was about 16 dB. Fig. 26 shows the PA's behavior when the supply voltage was varied. Also shown in Fig. 26 is a near linear relationship between output voltage and V_{DC}. By

decreasing V_{DC} from 32 to 14 V, the output power was reduced by 6.8 dB from 41.9 to 35.1 dBm, within which range the drain efficiency of at least 75% was achieved. Simulated output power spectrum is shown in Fig. 27.

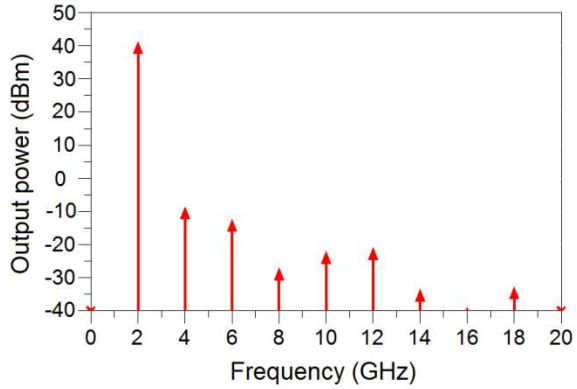

Fig. 27. Simulated output power spectrum of the FHP Class-EF PA.

C. Measurement Vs. Simulation

The THP Class-EF PA was designed to operate at 2.5 GHz. However, as can be seen from Fig. 28(a), the measured frequency shifted to a lower frequency, around 2.2 GHz. This disagreement is mainly due to the fact that the transistor model provided by the manufacturer does not incorporate packaged lead inductances at the gate and drain. When these inductances are included in the model, the simulation agrees pretty well with the measurement result, Fig. 28(b). The same applies to the FHP Class-EF PA where the design frequency is 2 GHz and measured frequency is 1.5 GHz, Fig. 29. The performances of the proposed PAs when compared to other published results are summarized in Table V. When compared with other PAs employing GaN HEMTs and operating at frequencies around 2 – 2.5 GHz [27]-[31], the THP Class-EF PA exhibits the highest drain efficiency and PAE at a comparable output power. The output power, drain efficiency, and PAE performances of the 1.52 GHz FHP Class-EF PA are superior to those of the 1.0 GHz PAs reported in [23]-[25].

VII. Conclusion

The analysis and design of THP and FHP Class-EF PAs including a method to increase their maximum operating frequency has been presented. These PAs employed a novel λ/8 open-circuit and shorted stub arrangement which facilitates improved even-harmonic suppression and therefore yields high efficiency. Since the FHP PA satisfies the Class-EF open-circuit load impedance requirement at not only $3f_0$ but also $5f_0$, its DC to RF efficiency is theoretically higher than that of the THP PA. However, in practice this might not be the case since the load network of the FHP PA is more sophisticated (thus more lossy), and prone to instability which in turn will degrade PA efficiency due to additional loss introduced by a stabilizing circuit.

The validity of the analytical derivation has been confirmed through harmonic-balance simulation and by measurement. Two PA prototypes were built using GaN HEMTs. The THP Class-EF PA delivered 39.5 dBm output power with 80% PAE at 2.22 GHz. Measured peak PAE of 81% and output power of 41.9 dBm were obtained at 1.52 GHz for the FHP Class-EF PA.

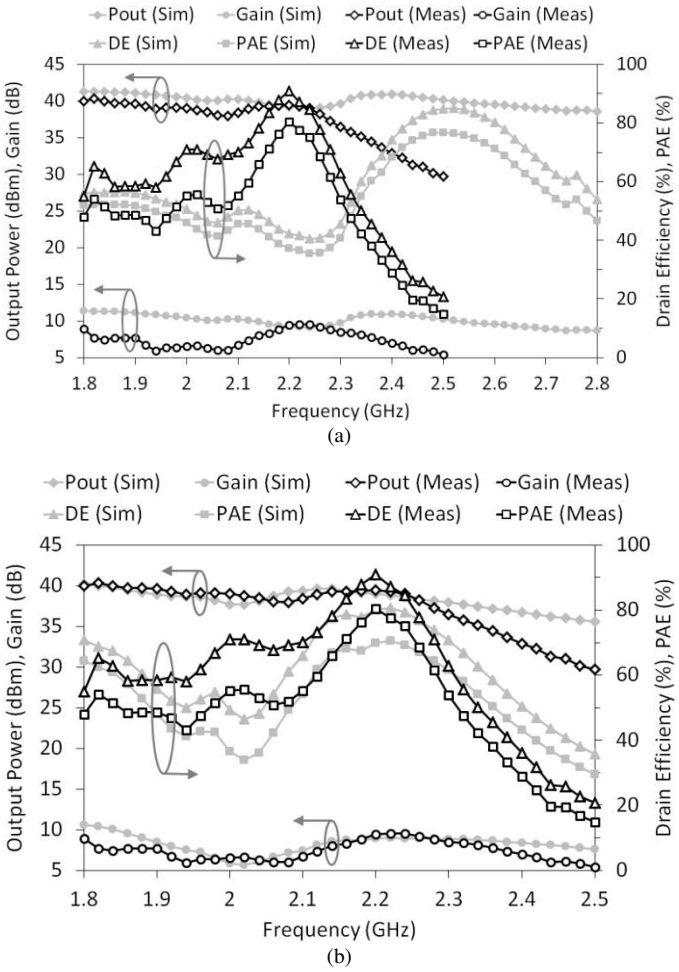

Fig. 28. Measured performances of the THP Class-EF PA compared with simulation results using: (a) original transistor model and (b) modified transistor model.

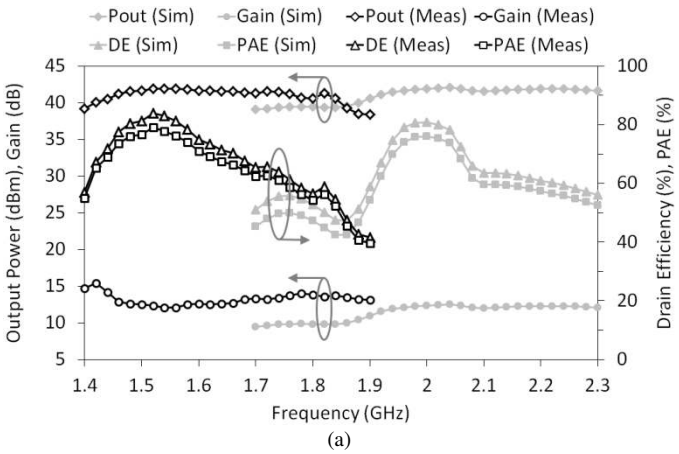

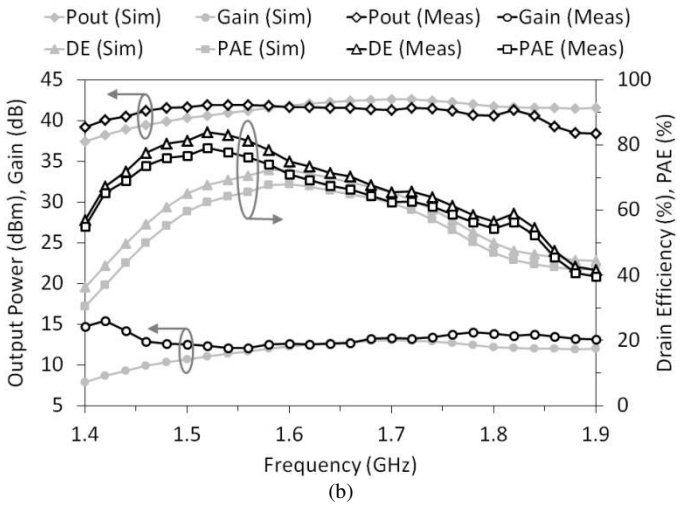

(b)

Fig. 29. Measured performances of the FHP Class-EF PA compared with simulation results using: (a) original transistor model and (b) modified transistor model.

TABLE V
PERFORMANCES SUMMARY AND COMPARISONS WITH OTHER PAS WITH OUTPUT POWER ≥ 2 W

Ref.	Freq. (MHz)	P_{OUT} (dBm)	η (%)	PAE (%)	Gain (dB)	V_{DC} (V)
[22][1]	61.44	33.7	86.6	85.7	19.7	10
[23]	1000	37	78.8	77.7	18.5	25
[24]	1000	39.8	77.5	74.2	13.7	28
[25]	1000	39.7	83.1	81.3	15.9	46
[26][1]	1000	41.5	76.7	75	16.5	50
[27]	2000	40.7	84.6	80.1	12.7	28
[28]	2140	40	76	73.1	14.3	30
[29]	2140	37	73	70	15	25
[30]	2450	39.4	-	71.2	-	28
[31]	2500	38.3	79	74	12	28
[32][2]	2550	34.7	72	64	9.5	8
[33]	3100	40	85	82	15	28
[34]	3475	38.4	83.1	80.1	14.4	28
[35]	3500	40.4	82	78	12	28
THP PA	**2220**	**39.5**	**91**	**80**	**9.2**	**28**
FHP PA	**1520**	**41.9**	**85**	**81**	**13.1**	**32**

[1] LDMOS, [2] GaAs pHEMT, otherwise GaN HEMT

REFERENCES

[1] S. C. Cripps, *RF Power Amplifiers for Wireless Communications*. Norwood, MA: Artech House, Inc., 2006.
[2] N. O. Sokal and A. D. Sokal, "Class E – A new class of high-efficiency tuned single-ended switching power amplifiers," *IEEE. J. Solid-State Circuits*, vol. 10, no. 3, pp. 168-176, Jun. 1975.
[3] F. H. Raab, "Idealized operation of the Class E tuned power amplifier," *IEEE Trans. Circuits Syst.*, vol. 24, no. 12, pp. 725-735, Dec. 1977.
[4] M. Thian, V. Fusco, and P. Gardner, "Power-combining Class-E amplifier with finite choke," *IEEE Trans. Circuits Syst. I*, *Reg. Papers*, vol. 58, no. 3, pp. 451-457, Mar. 2011.
[5] T. Mury and V. Fusco, "Exploring figures of merit associated with the suboptimum operation of Class-E power amplifiers," *IET Circuits Devices Syst.*, vol. 1, no. 6, pp. 401-407, Dec. 2007.
[6] T. Mury and V. F. Fusco, "Series-L/parallel-tuned comparison with shunt-C/series-tuned Class-E power amplifier," *IEE Circuits Devices Syst.*, vol. 152, no. 6, pp. 709-717, Dec. 2005.
[7] T. Mury and V. F. Fusco, "Sensitivity characteristics of Inverse Class-E power amplifier," *IEEE Trans. Circuits Syst. I*, *Reg. Papers*, vol. 54, no. 4, pp. 768-778, Apr. 2007.
[8] T. Mury and V. Fusco, "Inverse Class-E amplifier with transmission-line harmonic suppression," *IEEE Trans. Circuits Syst. I*, *Reg. Papers*, vol. 54, no. 7, pp. 1555-1561, Jul. 2007.
[9] F. H. Raab, "Class-F power amplifiers with maximally flat waveforms," *IEEE Trans. Microwave Theory Techn.*, vol. 45, no. 11, pp. 2007-2012, Nov. 1997.
[10] M. D. Weiss, F. H. Raab, and Z. Popovic, "Linearity of X-band Class-F power amplifiers in high-efficiency transmitters," *IEEE Trans. Microwave Theory Techn.*, vol. 49, no. 6, pp. 1174-1179, Jun. 2001.
[11] K. W. Eccleston, "Modified Class-F distributed amplifier," *IEEE Microw. Wireless Compon. Lett.*, vol. 14, no. 10, pp. 481-483, Oct. 2004.
[12] V. Carrubba, A. L. Clarke, M. Akmal, J. Lees, J. Benedikt, P. J. Tasker, and S. C. Cripps, "On the extension of the continuous Class-F mode power amplifier," *IEEE Trans. Microwave Theory Techn.*, vol. 59, no. 5, pp. 1294-1303, May 2011.
[13] A. Grebennikov and N. O. Sokal, *Switchmode RF Power Amplifiers*. New York: Newnes, 2007.
[14] T. Suetsugu and M. K. Kazimierczuk, "Comparison of Class-E amplifier with nonlinear and linear shunt capacitance," *IEEE Trans. Circuits Syst. I*, vol. 50, no. 8, pp. 1089–1097, Aug. 2003.
[15] S. D. Kee, I. Aoki, A. Hajimiri, and D. Rutledge, "The Class-E/F family of ZVS switching amplifiers," *IEEE Trans. Microwave Theory Techn.*, vol. 51, no. 6, pp. 1677-1690, Jun. 2003.
[16] J. W. Phinney, D. J. Perreault, and J. H. Lang, "Radio-frequency inverters with transmission-line input networks," *IEEE Trans. Power Electron.*, vol. 22, no. 7, pp. 1154-1161, Jul. 2007.
[17] A. Grebennikov, "High-efficiency Class-FE tuned power amplifiers," *IEEE Trans. Circuits Syst. I*, *Reg. Papers*, vol. 55, no. 10, pp. 3284-3292, Nov. 2008.
[18] J. M. Rivas, Y. Han, O. Leitermann, A. D. Sagneri, and D. J. Perreault, "A high-frequency resonant inverter topology with low-voltage stress," *IEEE Trans. Power Electron.*, vol. 23, no. 4, pp. 1759-1771, Jul. 2008.
[19] Z. Kaczmarczyk, "High-efficiency Class E, EF_2, and E/F_3 inverters," *IEEE Trans. Ind. Electron.*, vol. 53, no. 5, pp. 1584-1593, Oct. 2006.
[20] M. Thian and V. F. Fusco, "Analysis and design of Class-E_3F and transmission-line Class-E_3F_2 power amplifiers," *IEEE Trans. Circuits Syst. I*, *Reg. Papers*, vol. 58, no. 5, pp. 902-912, May 2011.
[21] M. Thian and V. Fusco, "High-efficiency low-voltage-stress Class-EF PA with extended maximum operating frequency," *German Microw. Conf.*, 2011, pp. 1-4.
[22] F. You, S. He, X. Tang, and X. Deng, "High-efficiency single-ended Class-E/F_2 power amplifier with finite DC feed inductor," *IEEE Trans. Microw. Theory Techn.*, vol. 58, no. 1, pp. 32-40, Jan. 2010.
[23] P. Aflaki, R. Negra, and F. M. Ghannouchi, "Design and implementation of an inverse class-F power amplifier with 79% efficiency by using a switch-based active device model," *IEEE Radio Wireless Symp.*, 2008, pp. 423–426.
[24] H. Kim, G. Choi, and J. Choi, "A high-efficiency inverse class-F power amplifier using GaN HEMT," *Microw. Opt. Technol. Lett.*, vol. 50, no. 9, pp. 2420–2422, Sep. 2008.
[25] M. Helaoui and F. M. Ghannouchi, "Optimizing losses in distributed multiharmonic matching networks applied to the design of an RF GaN power amplifier with higher than 80% power-added efficiency," *IEEE Trans. Microw. Theory Techn.*, vol. 57, no. 2, pp. 314–322, Feb. 2009.
[26] P. Singerl, C. Fager, Z. Wang, C. Schuberth, and F. Dielacher, "A highly efficient 1-GHz, 15-W power amplifier design based on a 50-V LDMOS transistor," *IEEE MTT-S Int. Microw. Symp.*, 2010, pp. 1102-1105.
[27] T. Hwang, et al., "Class-F power amplifier with 80.1% maximum PAE at 2 GHz for cellular base-station applications," *IEEE Wireless and Microw. Tech. Conf.*, 2013, pp. 1-3.
[28] A. Grebennikov, "High-efficiency Class E/F lumped and transmission-line power amplifiers," *IEEE Trans. Microw. Theory Techn.*, vol. 59, no. 6, pp. 1579-1588, Jun. 2011.
[29] A. Grebennikov, "High-efficiency transmission-line GaN HEMT inverse Class F power amplifier for active antenna arrays," *IEEE Asia-Pacific Microw. Conf.*, 2009, pp. 317-320.
[30] M. M. Ebrahimi, M. Helaoui, and F. M. Ghannouchi, "Efficiency enhancement of a WiMAX switching mode GaN power amplifier through layout optimization of distributed harmonic matching networks," *Eur. Microw. Conf.*, 2009, pp. 379-382.
[31] M. R. Ghajar and S. Boumaiza, "High efficiency GaN Class E amplifier for polar transmitter," *Int. Conf. on Signals, Circuits and Syst.*, 2009, pp. 1-4.

[32] G. F. Collins and J. Wood, "Class-E power amplifier design at 2.5 GHz using a packaged transistor," *IEEE Radio Wireless Symp.*, 2013, pp. 259-261.
[33] K. Chen and D. Peroulis, "A 3.1-GHz Class-F power amplifier with 82% power-added-efficiency," *IEEE Microw. Wireless Compon. Lett.*, vol. 23, no. 8, pp. 436-438, Aug. 2013.
[34] J. Moon, J. Lee, R. S. Pengelly, R. Baker, and B. Kim, "Highly efficient saturated power amplifier," *IEEE Microw. Mag.*, vol. 13, no. 1, pp. 125-131, Jan. 2012.
[35] P. Saad, H. M. Nemati, M. Thorsell, K. Andersson, and C. Fager, "An inverse class-F GaN HEMT power amplifier with 78% PAE at 3.5 GHz," *Eur. Microw. Conf.*, 2009, pp. 496-499.

Mury Thian obtained the B.Sc. degree from Atma Jaya Catholic University, Jakarta, Indonesia, the M.Sc. degree from Delft University of Technology, Delft, the Netherlands, and the Ph.D. degree from the Queen's University of Belfast, Belfast, United Kingdom, all in electronics engineering.

He was with Astra International ISUZU (Jakarta, Indonesia), NXP Semiconductors (Nijmegen, the Netherlands), the University of Birmingham (Birmingham, United Kingdom), and Infineon Technologies (Villach, Austria) before joining the Queen's University of Belfast (Belfast, United Kingdom) as a lecturer in 2013.

Dr. Thian has authored over 40 journal and conference papers and has co-authored two book chapters. He has been invited to chair sessions and give talks in a number of IEEE major conferences and workshops. He was a Marie Curie Fellow and the 2008 finalist of the British Association for the Advancement of Science.

Ayman Barakat (S'14) received the B.Sc. degree in electrical engineering from Ain Shams University, Cairo, Egypt, in 2005, and the M.Sc. degree in electrical engineering from Tampere University of Technology, Tampere, Finland, in 2013. He worked in the telecommunication and electrical industry from March 2006 to July 2013. He is currently an early stage researcher and working toward the PhD degree in electrical engineering at the Queen's University Belfast, Belfast, United Kingdom. His research interests include switched-mode and Doherty power amplifiers design for multiband transmitters.

Vincent Fusco (S'82-M'82-SM'96-F'04) obtained his Bachelor's degree in Electrical and Electronic Engineering (First Class Honours) and his Ph.D. in Microwave Electronics from the Queen's University of Belfast. Since 1995, he has held a personal chair in High Frequency Electronic Engineering.

His research interests include nonlinear microwave circuit design, and active and passive antenna techniques. The main focus for this research is in the area of wireless communications. At present he is technical director of the High Frequency Laboratories at ECIT (www.ecit.qub.ac.uk), where he is also director of the International Centre for Research for System on Chip and Advanced Micro-wireless Integration (SoCaM).

Prof. Fusco has published numerous scientific papers in major journals and in referred international conferences, and is the author of two text books. He holds several patents and has contributed invited chapters to books in the field of active antenna design and EM field computation. He is a Fellow of the Royal Academy of Engineering, a Fellow of the Institution of Engineering and Technology (IET), a Fellow of the Institute of Electrical and Electronic Engineers (IEEE), and of the Royal Irish Academy. In 1986, he was awarded a British Telecommunications Fellowship and in 1997 he was awarded the NI Engineering Federation Trophy for outstanding industrially relevant research.